SAND2015-8077J

Reduction-oxidation Enabled Glass-ceramics to Stainless Steel Bonding Part I: screening of doping oxidants

Steve Dai

Materials Science and Engineering Center
Sandia National Laboratories
Albuquerque, NM 87185-1349, USA

Abstract

Lithium silicate-based glass-ceramics with high coefficients of thermal expansion, designed to form matched hermetic seals in 304L stainless steel housing, show little evidence of interfacial chemical bonding, despite extensive inter-diffusion at the glass-ceramic-stainless steel (GC-SS) interface. A series of glass-ceramic compositions modified with a variety of oxidants, AgO, FeO, NiO, PbO, SnO, CuO, CoO, MoO_3 and WO_3, are examined for the feasibility of forming bonding oxides through reduction-oxidation (redox) at the GC-SS interface. The oxidants were selected according to their Gibbs free energy to allow for oxidation of Cr/Mn/Si from stainless steel, and yet to prevent a reduction of P_2O_5 in the glass-ceramic where the P_2O_5 is to form Li_3PO_4 nuclei for growth of high expansion crystalline SiO_2 phases. Other than the CuO and CoO modified glass-ceramics, bonding from interfacial redox reactions were not achieved in the modified glass-ceramics, either because of poor wetting on the stainless steel or a reduction of the oxidants at the surface of glass-ceramic specimens rather than the GC-SS interface.

Introduction

Lithium silicate glass-ceramics, usually modified with a small amount of other oxides (for example, K_2O, B_2O_3, Al_2O_3, ZnO, and often P_2O_5 as the high temperature nucleating agent) have been extensively used for sealing electrical feedthroughs in metal housings [1]. Glass-ceramic-to-metal (GCtM) seals combine the ease of conventional glass-to-metal (GtM) seals, as well as the performance often achieved in ceramic-to-metal (CtM) seals. The GCtM seals in particular offer several distinct advantages: high temperature mechanical strength of the seals, high dielectric breakdown strength for greater electrical isolation, good hermeticity for environmental protection, and long-term reliability. These unique properties enable GCtM seals to be widely adopted in high performance components and systems that are often deployed in extreme environments and for high-consequence and mission-critical applications.

The major crystalline phases formed in the lithium silicate system are lithium silicate (Li_2SiO_3), lithium disilicate ($Li_2Si_2O_5$) and silica polymorphs, i.e., Cristobalite, Quartz and Tridymite. Bulk crystallization occurring in this system is nucleated by Li_3PO_4 [2]. On heating, Li_2SiO_3 appears around 650 °C and then converts to $Li_2Si_2O_5$ around 850 °C by reaction with SiO_2 from the melt. Preheating the glass at 1000 °C dissolves the Li_2SiO_3 and $Li_2Si_2O_5$ crystals and forms heterogeneous Li_3PO_4 nuclei that promote crystallization of Li_2SiO_3, $Li_2Si_2O_5$ and Cristobalite on subsequent cooling of the melt. The crystallization occurs by epitaxial growth on favored facets of the Li_3PO_4 crystallites [3]. Depending on the type, as well as the amount of the crystallized phases, GCs with a moderate to high coefficient of thermal expansion (CTE) (10 - 18 ppm/°C) can be produced [4,5].

Glass Ceramic-Stainless Steel Interfacial Reactions

Two patented lithium silicate glass-ceramics, Li_2O-SiO_2-Al_2O_3-K_2O-B_2O_3-P_2O_5 (designated SB glass [6]), and Li_2O-SiO_2-Al_2O_3-K_2O-B_2O_3-P_2O_5-ZnO (designated as belt processable S-glass (BPS) glass-ceramic [7]), were developed to seal electrical feedthroughs to nickel-based and stainless steel (SS) alloys. The glass-ceramics are basically lithium silicate with additions of small amounts of other oxides (Table 1). In particular, high CTE BPS glass-ceramic was developed to form matched hermetic seals to high expansion low-carbon SS, such as 304L. After heat treatment, the glass-ceramics contain crystalline phases of nucleant Li_3PO_4, Li_2SiO_3, Cristobalite and a minor amount of $Li_2Si_2O_5$ and Quartz. The glass-ceramics also contain a residual glass phase rich in oxides of potassium, aluminum, zinc, and silicon.

Table 2 shows the composition of a typical 304L vacuum arc re-melt stainless steel. With very low carbon and sulfur, the stainless steel is optimized for welding performance. At 19.5 wt%, the Cr is much higher than the minimum 12 ~ 13 wt% required for oxidation resistance.

The interfacial reactions between the GC-SS are well known [8,9,10,11,12,13,14]. During the sealing process, Cr diffuses rapidly into glass-ceramic and is oxidized to form Cr_2O_3 crystals positioning in the glass-ceramics as deep as several 10s of μm from the GC-SS interface. Iron phosphate (Fe-P) compounds, due to iron diffusion into the glass-ceramic, are also observed, often next to or coexisting with the Cr_2O_3 crystals. On the other hand, a reduction of P_2O_5 in glass-ceramic and an accumulation of P near the GC-SS interface are also observed. Figure 1a is a SEM cross section image of a GC-SS interface. There is a distinct P depletion band along the

GC-SS interface in the mapping of P (Figure 1b). Several high P concentration areas indicate a clustering of P in the depletion band, as well as an accumulation of P at the GC-SS interface. The light-colored crystals in glass-ceramic next to the GC-SS boundary in Figure 1a clearly correlates to the Cr_2O_3, as confirmed by the Cr mapping in Figure 1c. The size of the Cr_2O_3 crystals is at 10 ~ 20 μm. In the SEM image, the Cr_2O_3 crystals exist at up to 40 μm into the glass-ceramic from the interface. In addition, a distance as far as 100 μm has also been observed. A close inspection of the Fe mapping in Figure 1d shows the co-existence of Fe and P clusters, which were further verified by high magnification SEM images as Fe-P compounds. The compounds are always seen in close proximity of the Cr_2O_3 crystals.

The fundamental driving force for the GC-SS interface reactions is the thermodynamically favorable reduction-oxidation (redox) where P_2O_5 serves as an oxidation agent and the Cr/Mn/Si is the reduction element. Table 3 lists standard Gibbs free energies in descending value for the formation of common oxides relevant to the this study. Group 1 lists candidate oxides for glass-ceramic modification (discussed in the experiment procedure section). It is clear that the Gibbs free energy of Cr_2O_3, MnO and all SiO_2 polymorphs in group 3, representing oxides of metal elements from stainless steel, are lower than those of group 2 P_2O_5 and ZnO in glass-ceramic. The difference in the Gibbs free energy is the driving force of the redox at the GC-SS interface, with the group 2 oxides being reduced for oxidation of metal elements in group 3.

During GCtSS sealing, the Cr, Mn and Si in stainless steel are readily oxidized as part of the interfacial redox. However, the Cr becomes the dominant reducing agent due to its high weight percentage. In the glass-ceramic, only P_2O_5 and ZnO could serve as the oxidation agents but the

reduction of P_2O_5 is much more thermodynamically favorable over that of ZnO. Iron diffusion from stainless steel into glass-ceramic is common in GCtM seals. However, in the current GC-SS system, the iron appears to combine to the reduced phosphor to form Fe-P compounds as the formation of Fe_2O_3 is thermodynamically unfavorable due to the relatively higher Gibbs free energy of Fe_2O_3 (Table 3).

Due to the depletion of P and thus, the inadequate formation of the Li_3PO_4 nuclei in glass-ceramic near the interface, a very course microstructure with large Li_2SiO_3 crystals are seen in the area. The region with P depletion and abnormal crystal growth is designated as the reaction zone in glass-ceramic. Studying the curvature of the stress-caused camber on a series of sequentially polished GC-SS samples by carefully removing glass-ceramic toward the interface, Kunz and Loehman [12] proved that the CTE of the reaction zone is lower than the CTE of the bulk glass-ceramic. The low CTE reaction zone may lead to tensile stress in the glass-ceramic, and was suggested as one of the possible causes for interfacial separation.

In the stainless steel, the depletion of Cr was found to be concentrated within 2 ~ 3 μm from the interface. Figures 2a and 2b show SEM cross sections of the GC-SS interface with a tapered cut and polish. The angle between the GC-SS interface and the polishing plane is 8º. The shallow polishing angle allowed an expanded view of the reaction zones with an amplification factor of about 7.2. Multiple Cr_2O_3 crystals are clearly visible in the reaction zone in the glass-ceramic in Figure 2a. The white needle-like spots on or near some Cr_2O_3 crystals are Fe-P compounds. The electron back-scattering (EBS) image on the stainless steel in Figure 2b shows well defined grains in bulk stainless steel but a very different morphology of the reaction zone near the

interface. Voids in grains and depleted grain boundaries exist throughout the reaction zone. Previous XRD work on the Cr depletion zone in stainless steel suggested the structure was body-centered cubic (bcc) at room temperature while the bulk stainless steel is face-centered cubic (fcc) [15,16]. The thin bcc layer, it was suggested, was formed on cooling from a high temperature fcc structure as a result of martensitic phase transformation in low Cr steels. The large volume change associated with the fcc-bcc phase transformation was believed detrimental to GC-SS seals because it produced higher stresses and a change of CTE near the interface [9].

One critical observation from all of the cross-sectional SEM images is the lack of chemical bonding, defined as an interfacial oxide adhesion layer, between the glass-ceramic and stainless steel. Despite the penetration of glass into the small pores and fine grain boundaries in the stainless steel and the inter-diffusion between the two materials, there is no evidence pointing to the existence of a distinct and continuous redox induced oxide layer at the interface.

Interfacial Bonding Oxide

It is well recognized that from a chemical or molecular approach, bonding must be accomplished by a transition zone in which the metallic bonding of the metal is gradually substituted for the ionic-covalent bonding of the glass [17,1]. Figure 3 illustrates the concept where a metal oxide layer is formed inside glass near the metal-glass interface. Strong chemical bonding can be achieved between a metal and a glass only if the conditions during bonding are such that the glass at the interface becomes and remains saturated with the appropriate metal oxide. Any effects that disrupt and erode this process may negatively impact the quality of the bond. It is

worth noting that strong chemical bonds may not form either when there is no such metal oxide present or when the metal oxide diffuses far into the glass without saturation at the interface.

The formation of interfacial oxides requires a source of oxygen. However, the atmosphere for GCtSS sealing needs to be inert, normally a flowing N_2 or Ar gas, to prevent oxidation of the stainless steel. In addition, the graphite, as the most common fixture material to avoid sticking to glasses and glass-ceramics, is chemically reducing in nature. For a GC-SS seal assembly held in graphite fixtures, there is essentially no oxygen available in the local atmosphere surrounding the glass-ceramics throughout a sealing cycle. These competing requirements, a need for oxygen to form an interfacial oxide bonding layer and a lack of oxygen inside the graphite fixture, limit the choice of forming bonding oxides to essentially two approaches: 1) pre-oxidation of SS to form surface oxides, typically C_2O_3, $MnCr_2O_4$ spinel and SiO_2 for 304L type stainless steel; or 2) doping of glass-ceramic with oxides to serve as oxidants to enable the interface redox reaction to form the bonding oxides. The current study is focused on the second scenario where pre-oxidation of the stainless steel housing is not an option, or it is undesirable in real applications.

Glass-Ceramic Modification

The goal of modifying glass-ceramics is to add metal oxides as "sacrificial" oxides, which could be reduced preferably over the P_2O_5 to preserve P_2O_5 for the formation of Li_3PO_4 nuclei. At the same time, the reduced metal may accumulate in glass-ceramic at the interface to form a barrier to block the diffusion of Cr and Fe from the stainless steel. In principle, any oxides having higher Gibbs free energy (for example, the oxides in Group 1 in Table 1) than that of P_2O_5 could serve the purpose. The criteria for a viable modification of glass-ceramic are the following: 1) The

metal oxides could be reduced, preferably over P_2O_5. 2) The metal ions of the dopants have the mobility to quickly diffuse to the interface; so kinetically, the redox is feasible. 3) The metal oxides need to be reduced at the GC-SS interface for redox reaction rather than at the free surfaces of the glass-ceramic because of the inert sealing atmosphere or even a reducing atmosphere inside the graphite fixture.

Experiment

Design and Fabrication of Modified Glass-Ceramics

The actual selection of oxides for glass-ceramic modification was based on multiple factors, including the Gibbs free energy, ease of processing the glass-ceramic, cost, and the environmental, safety and health (ESH) impact. Each glass-ceramic composition was batched at 1.5 kg weight. The mixed raw oxide materials were melted in a platinum crucible at 1550 ºC with extensive stirring. The molten glass was cast to disc ingots at a diameter about 2 inches and thickness 0.25 to 0.50 inch. All modified glass-ceramics were fabricated by Ceradyne Viox Inc. (Seattle, USA), which is now a division of 3M Corp.

Table 4 lists Viox-produced BPS_base glass-ceramic (composition from Table 3) and modified glass-ceramic compositions based on the BPS formulation. Each added oxide was balanced by the same weight reduction on SiO_2. The BPS_Zn, with more than double the wt% of the original ZnO, was designed to study whether the extra ZnO could enhance the redox reaction with Cr from stainless steel. The idea was to test whether the relative higher wt% of ZnO could shield P

in glass-ceramic, although thermodynamically, the reduction of P_2O_5 is more favorable. An analogy is the preferred oxidation of Cr over Mn and Si from stainless steel due to the high weight percentage of Cr, although the formation of Cr_2O_3 was less thermodynamically favorable. The BPS_Co1 and BPS_Co2 with 0.50 and .99 wt% CoO were fabricated because: 1) The Gibbs free energy of CoO is lower than that of P_2O_5, and 2) the small amount of CoO doping was one of the most commonly used methods to promote the adhesion of glass and glass ceramics to metals. CuO modification is attractive due to the even lower formation energy of CuO (compering to CoO) and the reported accumulation of Cu near the GC-SS interface [8].

Modified glass-ceramics based on SB glass-ceramic are listed in Table 5. All of the dopant metal oxides belong to Group 1 in Table 3 and have higher Gibbs free energy than that of P_2O_5. The amount of oxide is fixed at 1 mol% with an exception of CoO modified glass-ceramics where a composition with 2 mol% CoO was fabricated. The CuO-doped glass-ceramics were formulated at a finer scale. Table 6 shows a formulation of base SB glass-ceramic and the compositions up to 1 mol% CuO at an increment of 0.25 mol% of CuO.

Finally, a few glass-ceramics doped with two oxidants were fabricated (Table 7). The purpose of composition SB050Cu050Co was to learn the combined redox effect from CoO and CuO. The formation of SB100Cu100Pb allowed examining the combined redox from CuO and PbO, as well as the effect of the anticipated decrease in glass-ceramic viscosity on the wetting behavior with the addition of PbO.

Characterization Methods

Sessile Drop Tests: The sessile drop technique is a method used for characterizing solid surface energies and, in some cases, aspects of liquid surface energies. It provides a simple, yet effective way to evaluate GC-SS interactions. In addition to studying the wetting behavior of a liquid droplet on a solid substrate by measuring wetting angles, the method is also used to assess the adhesion between glass-ceramics and stainless steel. There is no bonding between the glass-ceramics and stainless steel when a glass-ceramics bead pops off from the stainless steel coupon after a sealing schedule. If the glass-ceramics adhered to stainless steel after a heat treatment, then the glass-ceramcis is considered bonded to the stainless steel, although the nature of adhesion requires a closer look of the interface.

The glass-ceramics for sessile drop study could be in any forms, for example, pressed powder preforms (PPPs), pieces of flake, chunks cut from as-cast glass ribbon or ingot, or even piles of glass-ceramics powder. Stainless steel coupons can be in different forms too, as long as there is enough flat surface area for glass-ceramics samples. The finish of stainless steel surface for sessile drop tests was at roughness average (Ra) 32 μInch. Often different glass-ceramics samples were tested on the same stainless steel coupon for a direct comparison of wetting and adhesion behavior.

GC –SS Bonding Assessment: Stainless steel pins at diameter 0.098 inch and lengths 0.5 or 1.0 inch with a Ra 32 finish on the end surfaces were used for glass-ceramic bonding tests. The pins were selected to meet a number of requirements and tested in different configurations: 1) a defined surface contact area on stainless steel, 2) glass-ceramic specimens placed on top a

standalone pin or GC-pin inside a graphite tube with an ID at 0.100 inch, and 3) glass-ceramics specimens sandwiched between two pins (pin-GC-pin) that are placed inside a through hole in the graphite tube. All configurations allow for a pull test on the GC-pin to assess the bonding strength. Figure 4 shows four GC-pin arrangements, and the graphite through hole fixture and end caps. The GC-pin can be placed inside or outside the graphite through hole with or without caps to test the effect of different local atmosphere. For bonding tests, the sandwiched pin-GC-pin assemblies need to be held inside the graphite fixture for thermal processing. The use of graphite tube and caps also simulates the local atmosphere in real fixtures for GCtSS seals.

For a qualitative test on the strength of the GC-SS bond, a bonded GC-SS was placed in a temperature chamber and shocked with liquid nitrogen. The sample was inspected after each of the setting temperatures -50 ºC, -100 ºC and -150 ºC to see whether the GC detached from or remain bonded to the stainless steel. Cooling to a set temperature is rapid, typically > 100 ºC/min with liquid nitrogen pouring directly over the samples.

Effect of Local Atmosphere:

A bell-style loading furnace (model# APF-0716-1800MM by Astro Industries Inc.) with molybdenum wire mesh heating elements was used for the entire GC-SS sealing, sessile drop and GC-pin bonding experiments. A circular molybdenum sheet shielded the center heating zone from the furnace's in-wall water-cooled outer steel chamber. In a sealing run, the furnace was initially pumped down to a pressure of about 242 mTorr and then filled with flowing N_2 or Ar to +5 Psig pressure. A Honeywell DCP-77001 controller fully automated the atmosphere sequence and temperature profile.

The oxygen partial pressure PO_2, measured by an oxygen sensor (OxyMaster 16TDP) through a sealing cycle using house N_2 as the process gas, is shown in Figure 5. During an initial waiting period, the PO_2 decreases rapidly. When the temperature starts rising, the PO_2 decreases approximately to around 10 ppm, and continues to drop as time goes by. At the peak sealing temperature around 1000 ºC, the PO_2 is in the range of 6 - 8 ppm. By the end of the sealing cycle, the PO_2 reaches ~ 3 ppm. The insert in Figure 5 shows an expanded PO_2 versus temperature plot. There is always residual oxygen in the furnace during sealing, although house N_2 is used as a process gas.

Results and Discussion

1. Initial screening of GC-SS bonding

Cubes at 0.067 by 0.067 by 0.067 inches were machined from all glass-ceramics and subject to sessile drop tests on stainless steel coupons sitting in alumina crucibles. The glass-ceramics were exposed to flowing N_2 during the sessile drop tests. The test configuration represented the most favorable condition for GCtSS adhesion because of the slight oxidation of the stainless steel by the trace amount of oxygen in N_2. It was observed consistently that if a glass-ceramic did not adhere to stainless steel in this test setup, it would not bond to the stainless steel in a reducing atmosphere — for example, inside a graphite fixture —, due to the absence of surface oxide on the stainless steel.

A bonding test of a glass-ceramic sandwiched vertically between two stainless steel pins inside a through hole of the graphite fixture (Figure 4) represented the least favorable condition for

GCtSS adhesion because of the reducing atmosphere. If a glass-ceramic could bond to the stainless steel in this configuration, it would very likely bond to the stainless steel under other process conditions. In actual GCtSS seal assemblies, the glass-ceramic PPPs inside stainless steel housing were supported by underneath graphite inserts. The feedthrough pins were held in place by the graphite inserts seated in a steel plate placed on top of the stainless steel housing. The local atmosphere around a glass-ceramic was primarily reducing in nature due to the presence of the graphite fixture.

In sessile drop tests, a glass-ceramic is considered wet to stainless steel when the wetting angle is less than 90 degrees. Figures 6a and 6b show SB_base and BPS_base glass-ceramics wetting the stainless steel. The SB_base glass-ceramics fell off the stainless steel coupon after testing, while the BPS_base glass-ceramics stayed bonded. Pin bonding tests of glass-ceramics in a graphite fixture showed that SB_base glass-ceramics fall off from both pins (Figure 6a), and the BPS_base glass-ceramics bonded to at least one pin (Figure 6b). It appeared that the ZnO in the BPS_base glass-ceramic improved the bonding to the stainless steel.

The modified glass-ceramics were also evaluated for surface appearance. A discolored surface indicated an accumulation of a metal from glass-ceramic. Part or all of the doped oxidant may be reduced at the glass-ceramic surface rather than being consumed for redox at the interface. For example, Figure 7 showes discolored WO_3 doped glass-ceramic SB_W on stainless steel. The SB_W glass-ceramic wet and bonded well to the stainless steel; it probably benefited from a redox at the GC-SS interface. However, the darkening of the glass-ceramic surface suggests that part of the WO_3 was reduced at the glass-ceramic surface exposed to flowing N_2. Also the degree

and location of surface darkening varied. For the glass-ceramic drop at the low-left positon on the stainless steel, the surface was nearly all darkened. For the same glass-ceramic drop sitting at the top-center position of the stainless steel, only the side walls turned dark, while the top square surface remained un-discolored.

Table 8 lists the results of two tests used to evaluate all glass-ceramics: 1) sessile drop tests with glass-ceramics and stainless steel coupons open to furnace N_2, and 2) pin bonding tests, in a vertical pin-GC-pin configuration, inside the though hole of a graphite fixture. The inspection on sessile drop samples included the wetting of glass-ceramics on stainless steel, GCtSS adhesion, and surface discoloring of the glass-ceramics. All sessile drop images are shown in Figure 8. The examination of the pin bonding samples focused on the bonding of a glass-ceramic to the pins and the discoloring of the side wall of the sandwiched glass-ceramic. Attention was also paid to the GC-SS interfacial reaction, which was revealed by a darkened reaction zone near the interface for bonded glass-ceramic or the detached interfaces for un-bonded glass-ceramics.

The judgment on the test results was presented by a Yes or No. In some cases more detailed information was provided, for example “bond to one pin” under the “bonding” column. The comment section highlighted unique observations of each test that were not captured by the Yes/No category.

The observations were also color coded: green meant favorable, red unfavorable. A glass-ceramic with all green marks had the potential to bond to SS and was subjected to further detailed investigation. Of all the compositions, the CoO-modified glass-ceramics stand out as the

most promising glass-ceramics to bond to stainless steel. The corresponding GCtSS interface was characterized extensively. A detailed study was also conducted on CuO-modified glass-ceramics as verified by two observations: 1) redox at the CuO-GCs and stainless steel interface was distinct at the right processing conditions, 2) a strong interfacial oxide bonding layer could be formed if the redox could proceed.

No further examinations were conducted on other modified glass-ceramics due to either the lack of adhesion in sessile drop and pin bonding tests, or excessive reduction of the oxidants at the glass-ceramic surface instead of the redox at the GC-SS interface. For glass-ceramics showing reduction of the oxidants at the surface in sessile drop tests where there was slight oxygen in the flowing N_2, the situation was expected to be worse for glass-ceramic in real GCtSS seals using the graphite fixture: the local atmosphere in the graphite fixture was reducing in nature. An oxidant was expected to be reduced more likely at the surface of glass-ceramic in a graphite fixture than glass-ceramic exposed to the flowing N_2.

Conclusions

A comprehensive survey on the bonding of modified lithium silicate glass-ceramics to stainless steel was conducted. The glass-ceramics were doped by common transition metal oxides to serve as oxidants for the intended interfacial redox reactions. Sessile drop tests were used to screen the glass-ceramics for wetting and adhesion to stainless steel. The GC-SS bonding was assessed by bonding tests in GC-pin and pin-GC-pin configurations inside graphite fixtures. Out of all modified glass-ceramic compositions, the CuO and CoO doped glass-ceramics showed strong

bonding to stainless steel. Bonding from interfacial redox reactions were not achieved in all other modified glass-ceramics, either because of poor wetting on the stainless steel or a reduction of the oxidants at the surface of glass-ceramic specimens rather than the GC-SS interface.

Acknowledgement

The authors would like to thank Dr. Don Susan for insightful discussions on GC-SS interactions. This work was supported by the Laboratory Directed Research and Development program at Sandia National Laboratories, a multi-program laboratory managed and operated by Sandia Corporation, a wholly owned subsidiary of Lockheed Martin Corporation, for the U.S. Department of Energy's National Nuclear Security Administration under contract DE-AC04-94AL85000.

References

1 Donald I. Glass-to-Metal Seals. Society of Glass Technology; 2009.

2 Hammetter WF, Loehman RE. Crystallization Kinetics of a Complex Lithium Silicate Glass-Ceramoc. Journal of American Ceramcis Society. 1987;70(8):577-582.

3 Headley TJ, Loehman RE. Crystallization of a Glass-Ceramic by Epitaxial Growth. Journal of teh Anerican Ceramics Society. 1984;67(9):620-624.

4 Henderson WR, Kramer DP, Sullenger DB. Determinination of the Optimum Crystallization Conditions of a High Thermal Expansion Glass-Ceramic. Miamiaburg, OH: Monsanto Research Corp; 1984 Monsanto Research Corp. MLM-3136.

5 Loehman RE, Headley TJ. Design of High Thermal Expansion Glass-Ceramcis. In: Pask JA, Evans AG, editors. Ceramic Microstructure'86; 1987. p. 33-43.

6 McCollister HL, Reed ST, inventors. Glass Ceramic Seals to Inconel. 1983. US4414282.

7 Reed S, Stone RG, McCollister HL, Wengert PR, inventors. Method of Processing "BPS" Glass Ceramic and Seals Made Therewith. 1998 Nov. US5820989.

8 Donald IW. Preparation, Properties, and Chemistry of Glass and Glass-ceramic-to-metal Seals and Coating. Journal of the American Ceramic Society. 1993 2849.

9 Knorovsky GA, Brow RK, Watkins RD, Loehman RE. Interfacial Debonding in Stainless Steel/Glass Ceramic Seals. Albuquerque: Sandia National Laboratories; 1989. SAND89-1866C.

10 Loehman RE. Processing and Interfacial Analysis of Glass-Ceramic to Metal Seals. Vol 4. American Society of Mechanical Engineers; 1987.

11 Watkins RD, Loehman RE. Interfacial Reaction Between a Complex Lithium Silicate Glass-Ceramic to Metal Seals. Advanced Ceramic Materials. 1986;1(1):77-80.

12 Kunz SC, Loehman RE. Thermal Expansion Mismatch Produced by Interfacial Reactions in Glass-Ceramic to Metal Seals. Advanced Ceramic Mateirals. 1986;2(1):69-73.

13 Benisu M, Brow RK, White JE. Interfacial Reaction Between Lithium Silicate Glass-Ceramics and Ni-Based Superalloys and the Effect of Heat Treatment at Elevated Temperatures. Journal of Materials Science. 2004 505-518.

14 Loehman RE. Interfacial Reaction in Ceramic-Metal Systems. Ceramic Bulletin. 1989;68(4):891-896.

15 Susan DF, Knorovsky GA, Robino CV, Michael JR, Rodriguez MA, Perricone MJ. Surface alloy depletion and martensite formation during glass to metal joining of austenitic stainless steels. Science and Technology of Welding and Joining. 2012;17(4):321-332.

16 Susan DF, Van Den Avyle JA, Monroe SL, Sorensen NR, McKenzie BB, Christensen JE. The Effects of Pre-Oxidation and Alloy Chemistry of Austenitic Stainless Steels on Glass/Metal Sealing. Oxidation of Metals. 2009;73(1-2):311-335.

17 Donald IW, Metcalfe BL, Gerrard LA. Interfacial Reactions in Glass-Ceramic-to-Metal Seals. Journal of Amewrican Ceramic Society. 2008;91(3):715 - 720.

Tables

Table 1. Composition of SB and BPS Glass-ceramics [6,7].

Table 2. Composition of 304L Stainless Steel.

Table 3. Standard Gibbs Free Energy per Mole of O_2.

Table 4. Modified Glass-ceramic Compositions Based on BPS Formulation.

Table 5. Glass-ceramics Based on SB Glass Formulation.

Table 6. CuO-modified Glass-ceramics Based on SB Glass Formulation.

Table 7. Glass-ceramics with Multiple Dopants.

Table 8. Summary of Sessile Drop Tests open to N_2 and Pin Bonding Tests in Graphite Fixture of Glass-ceramics.

Figure Captions

Figure 1. SEM cross section of GC-SS interface: (a) grey image, (b) P map, (c) Cr map, and (d) Fe map.

Figure 2. Amplified SEM view of, a) reaction zone in glass-ceramic with Cr_2O_3 course Li_2SiO_3 crystals, and b) EBS image showing the Cr depleted reaction zone in stainless steel.

Figure 3. Schematic representation of chemical bonding between glass and metal.

Figure 4. Graphite fixture for pin test and GC-pin configurations.

Figure 5. Oxygen partial pressure PO_2 in a sealing cycle with N_2 as processing gas. The insert shows expanded view of PO_2.

Figure 6. Images of (a) SB_base and (b) BPS_base glass-ceramics from sessile drop test open to furnace N_2 and pin bonding test in graphite fixture.

Figure 7. Discoloring of SB_W glass-ceramic indicated WO_3 being reduced at the surface.

Figure 8. Sessile drop of all glass-ceramic specimens.

Table 1. Composition of SB and BPS Glass-ceramics [6,7].

Oxide	SB GC (wt%)	BPS GC (wt%)
SiO_2	74.32	74.40
Li_2O	13.02	12.65
Al_2O_3	4.66	3.80
K_2O	4.04	2.95
B_2O_3	1.38	1.20
P_2O_5	2.58	3.15
ZnO		1.85

Table 2. Composition of 304L Stainless Steel

Element	Wt%	Element	Wt%
Fe	67.41	S	0.003
Cr	19.49	P	0.018
Ni	10.34	C	0.017
Mn	1.77	Nb	0.017
Si	0.62	N	0.01
Cu	0.13	Al	0.006
Mo	0.12	Ti	0.002
Co	0.05	O	0.001

Table 3. Standard Gibbs Free Energy per Mole of O_2.

Oxidation Reaction	Gibbs Free Energy ($\Delta G°$, kJ/mol O_2, 25 °C)	Note
$4Ag + O_2 = 2Ag_2O$	-22	Group 1: Candidates for dopant oxides in GC as oxidants for preferred reduction over P_2O_5 to form interfacial bonding oxides by redox
$2Cu_2O + O_2 = 4CuO$	-219	
$2MoO_2 + O_2 = 2MoO_3$	-275	
$4Cu + O_2 = 2Cu_2O$	-289	
$2Pb + O_2 = 2PbO$	-379	
$2Co + O_2 = 2CoO$	-425	
$2Ni + O_2 = 2NiO$	-430	
$2/3Mo + O_2 = 2/3MoO_3$	-445	
$2Fe + O_2 = 2FeO$	-482	
$4/3Fe + O_2 = 2/3Fe_2O_3$	-495	
$2W + O_2 = WO_2$	-505	
$2/3W + O_2 = 2/3WO_3$	-509	
$Mo + O_2 = MoO_2$	-530	
$Sn + O_2 = SnO_2$	-535	
$6FeO + O2 = 2Fe_3O_4$	-549	
$4/5P + O_2 = 2/5P_2O_5$	-572	Group 2: Existing oxidants in GC
$2Zn + O_2 = 2ZnO$	-636	
$4/3Cr + O_2 = 2/3Cr_2O_3$	-695	Group 3: Alloying elements in SS as reducing agents
$2Mn + O_2 = 2MnO$	-726	
$Si + O_2 = SiO_2$, quartz	-856	
$Si + O_2 = SiO_2$, cristobalite	-856	
$Si + O_2 = SiO_2$, tridymite	-855	
$Si + O_2 = SiO_2$, quartz glass	-851	

Table 4. Modified Glass-ceramic Compositions Based on BPS Formulation.

Oxides	BPS_base (wt%)	BPS_Zn (w%)	BPS_Co1 (w%)	PBS_Co2 (wt%)	BPS_Cu1 (wt%)	BPS_Cu2 (wt%)
SiO_2	74.35	72.2	73.98	73.61	72.95	72.35
Li_2O	12.70	12.7	12.64	12.57	12.55	12.7
Al_2O_3	3.80	3.8	3.78	3.76	3.79	3.8
K_2O	2.95	2.95	2.94	2.92	3.00	2.95
B_2O_3	1.20	1.2	1.19	1.19	1.17	1.2
P_2O_5	3.15	3.15	3.13	3.12	3.27	3.15
ZnO	1.85	4.0	1.84	1.83	1.85	1.85
CoO			0.5	0.99		
CuO					1.41	2.0

Table 5. Glass-ceramics Based on SB Glass Formulation.

Oxides	SB_Pb (w%)	SB_Ni (w%)	SB_Fe (w%)	SB_Ag (wt%)	SB_Sn (wt%)	SB_W (wt%)	SB_Mo (wt%)	SB_Co1 (wt%)	SB_Co2 (wt%)
SiO_2	72.81	74.74	74.78	74.09	73.95	72.71	73.83	74.74	73.47
Li_2O	12.3	12.62	12.63	12.51	12.49	12.28	12.47	12.62	12.59
Al_2O_3	3.72	3.82	3.82	3.78	3.78	3.71	3.77	3.82	3.81
K_2O	2.94	3.02	3.02	3.00	2.99	2.94	2.98	3.02	3.01
B_2O_3	1.15	1.18	1.18	1.17	1.17	1.15	1.16	1.18	1.18
P_2O_5	3.2	3.29	3.29	3.26	3.25	3.20	3.25	3.29	3.28
Dopant	3.88	1.33	1.28	2.19	2.38	4.02	2.53	1.34	2.66
Note	1 mol% PbO	1 mol% NiO	1 mol% FeO	1 mol% AgO	1 mol% SnO	1 mol% WO_3	1 mol% MoO_3	1 mol% CoO	2 mol% CoO

Table 6. CuO-modified Glass-ceramics Based on SB Glass Formulation.

Oxides	SB_base (wt%)	SB025Cu (w%)	SB050Cu (w%)	SB075Cu (wt%)	SB100Cu (wt%)
SiO_2	76.01	75.68	75.13	75.00	74.67
Li_2O	12.65	12.64	12.81	12.63	12.61
Al_2O_3	3.83	3.82	3.82	3.82	3.81
K_2O	3.03	3.03	3.03	3.02	3.02
B_2O_3	1.18	1.18	1.18	1.18	1.18
P_2O_5	3.30	3.29	3.32	3.29	3.29
CuO		0.36	0.71	1.06	1.42
Note		0.25 mol% CuO	0.50 mol% CuO	0.75 mol% CuO	1.00 mol% CuO

Table 7. Glass-ceramics with Multiple Dopants.

Oxides	SB050Cu050Co (wt%)	SB100Cu100Pb (wt%)
SiO_2	74.71	71.53
Li_2O	12.61	12.25
Al_2O_3	3.81	3.71
K_2O	3.02	2.93
B_2O_3	1.18	1.14
P_2O_5	3.29	3.19
CuO	0.71	1.38
CoO	0.67	
PbO		3.86
Note	0.5 mol% CoO and 0.5 mol% CuO	1.0 mol% PbO and 1.0 mol% CuO

Table 8. Summary of Sessile Drop Tests open to N_2 and Pin Bonding Tests in Graphite Fixture of Glass-ceramics.

Glass-ceramic	Sessile Drop Test in Furnace N_2			Comment	Pin in Graphite fixture		Comment
	Wetting	Adhesion	Surface discoloring		Bonding	Side wall discoloring	
BPS_base	Yes	Yes	N/A	Interfacial reactions. Adhesion in consistent.	Bond to one pin	N/A	Interfacial reaction with Cr diffusing to GC
BPS_Zn	Yes	Yes	N/A	Similar to the original BPS	No	N/A	No bond to either pins
BPS_Co1	Yes	Yes	No	BPS_Co1 wets better than BPS_Co2. Good Candidate	Yes	No	Bonded, but easily break off
PBS_Co2	Yes	Yes	No	Candidate for interfacial redox	Yes	No	Bonded. Can survive handling.
BPS_Cu1	Limited	Half/half	Partial	Some CuO reduction at the GC surface	No	Yes	Some CuO reduction at the GC sruface
BPS_Cu2	Yes	Yes	Yes	CuO reduction at GC surface	No	Yes	CuO reduction at GC surface and GC-SS interface due t excessive CuO
SB_base	Yes	No	N/A	Worse than BPS_base?	No	N/A	No bond to either pins
SB025Cu	Yes	No	Partial	Similar to SB_base	Bonded to 1 pin	No	Bonded to one pin but de-bonded from the other
SB050Cu	Yes	No	Yes	CuO reduced at surface	½ pins bonded	Some	Two out of four Pin-GC-Pin bonded.
SB075Cu	Yes	Yes	Yes	CuO reduced at surface	Yes	Some	Cu on side wall. More near interface
SB100Cu	Yes	Yes	Yes	CuO reduced at surface	Yes	Yes	Side face saturated with Cu
SB_Pb	Yes	Yes	No	Potential ESH concerns on Pb	No	No	No boding at all. PbO not reduced
SB_Ni	Yes	No	Yes	NiO reduced at surface	No	Yes	NiO reduced at the GC side face
SB_Fe	Yes	No	Yes	FeO reduced at surface	Bonded to 1 pin	Yes	Heavy reduction of FeO at side face
SB_Ag	Partial	Partial	Yes	AgO reduced at surface	No	Yes	Poor wetting. AgO reduced at surface
SB_Sn	Yes	No	No	Poor adhesion	No	No	No adhesion and bonding
SB_W	Yes	Yes	Yes	WO_3 reduce at surface	No	Yes	Heavy reduction a the GC side face
SB_Mo	Yes	Yes	Yes	MoO_3 reduce at surface	No	Yes	Heavy reduction a the GC side face
SB_Co1	Yes	No	No	Poor adhesion due to low wt% of CoO	No	No	Poor adhesion and bonding due to not enough CoO
SB_Co2	Yes	Yes	No	Candidate as modified GC for interfacial redox	Yes	No	Promising composition.
SB050Cu050Co	Yes	Yes	Yes	CuO reduced at surface	Yes	Minor	Good. CuO surface reduction an issue
SB100Cu100Pb	Yes	Yes	Yes	CuO reduced at surface	No	Yes	Did not bond any pin. CuO reduced at side surface showing Cu

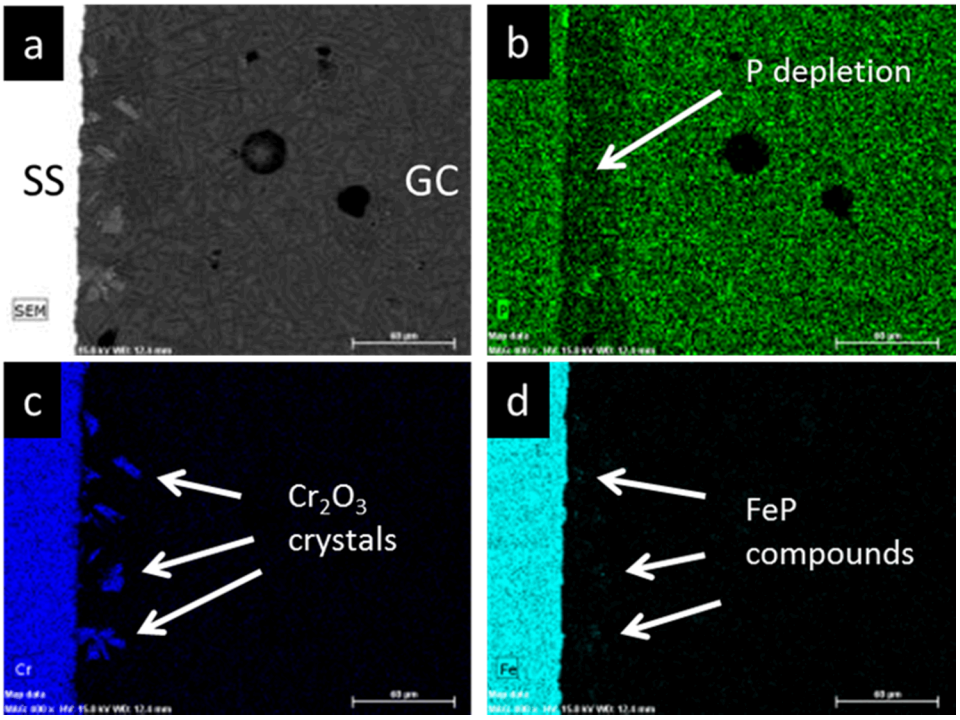

Figure 1. SEM cross section of GC-SS interface: (a) grey image, (b) P map, (c) Cr map, and (d) Fe map.

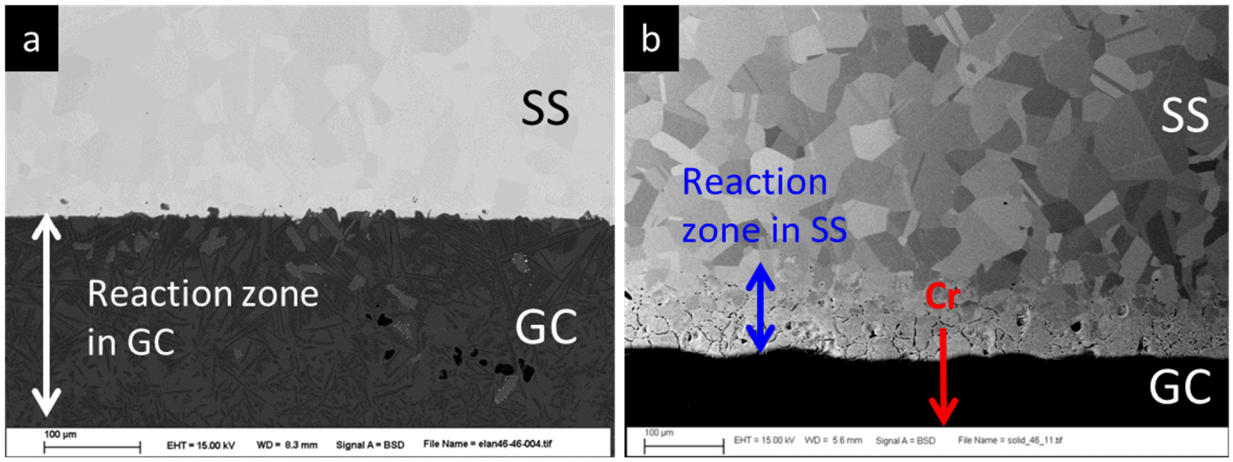

Figure 2. Amplified SEM view of, a) reaction zone in glass-ceramic with Cr_2O_3 course Li_2SiO_3 crystals, and b) EBS image showing the Cr depleted reaction zone in stainless steel.

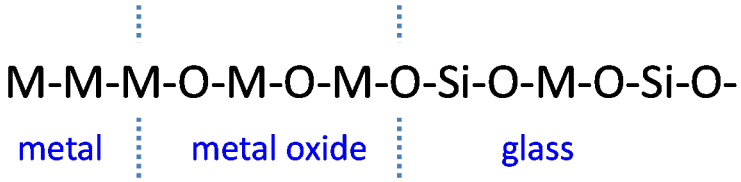

Figure 3. Schematic representation of chemical bonding between glass and metal.

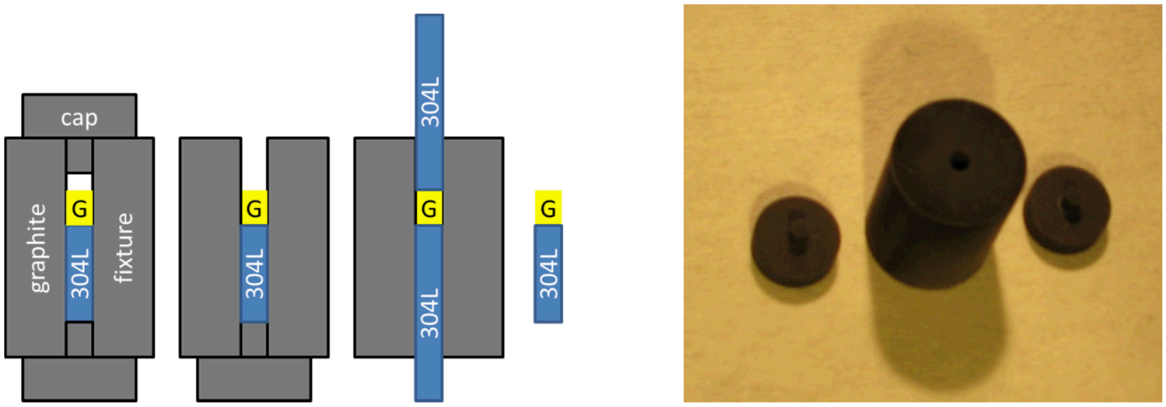

Figure 4. Graphite fixture for pin test and GC-pin configurations.

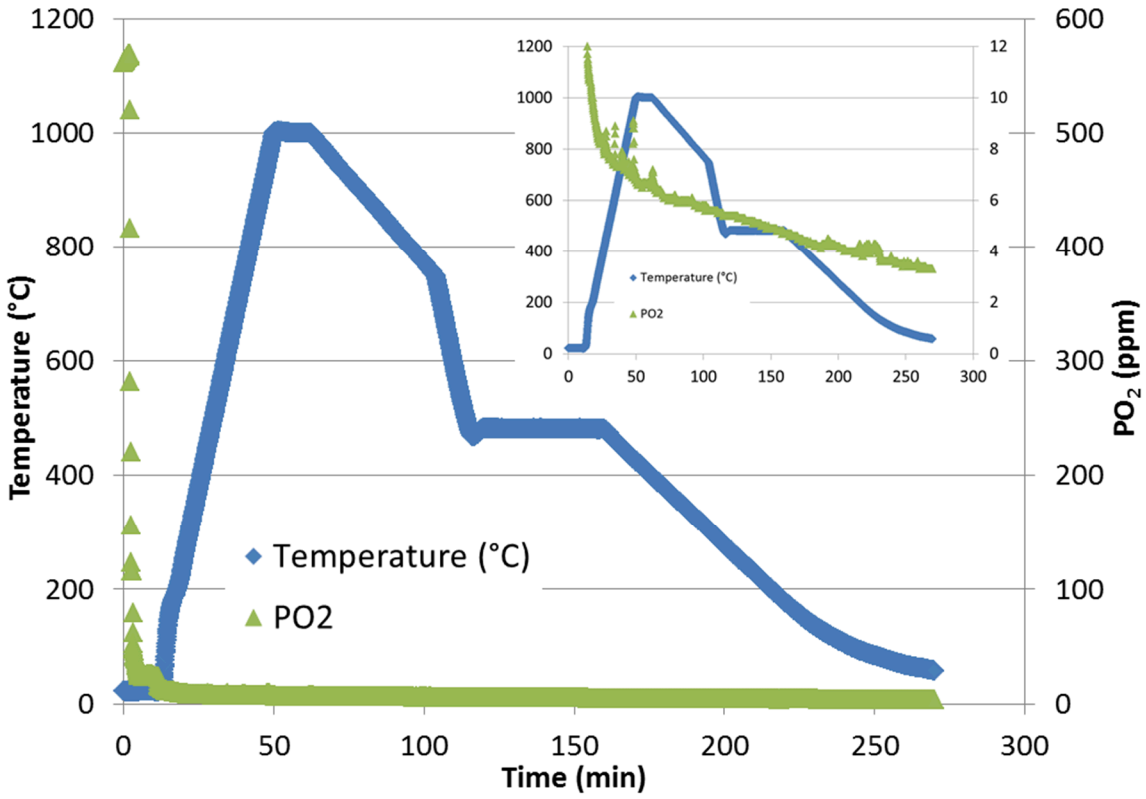

Figure 5. Oxygen partial pressure PO_2 in a sealing cycle with N_2 as processing gas. The insert shows expanded view of PO_2.

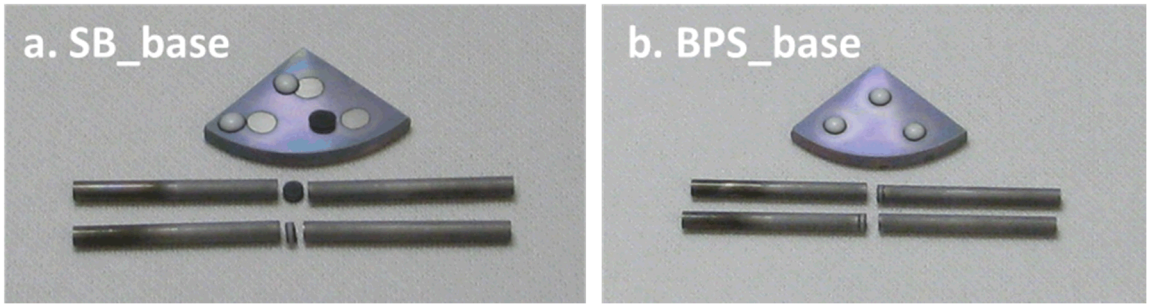

Fig 6. Images of (a) SB_base and (b) BPS_base glass-ceramics from sessile drop test open to furnace N_2 and pin bonding test in graphite fixture.

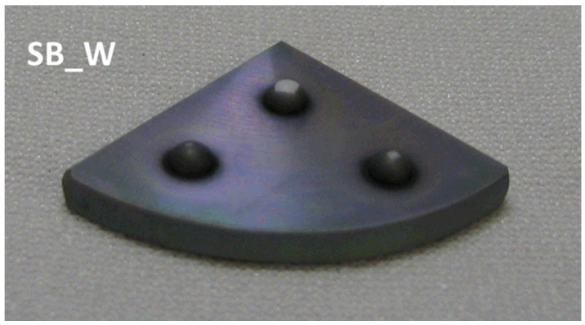

Fig 7. Discoloring of SB_W glass-ceramic indicated WO_3 being reduced at the surface.

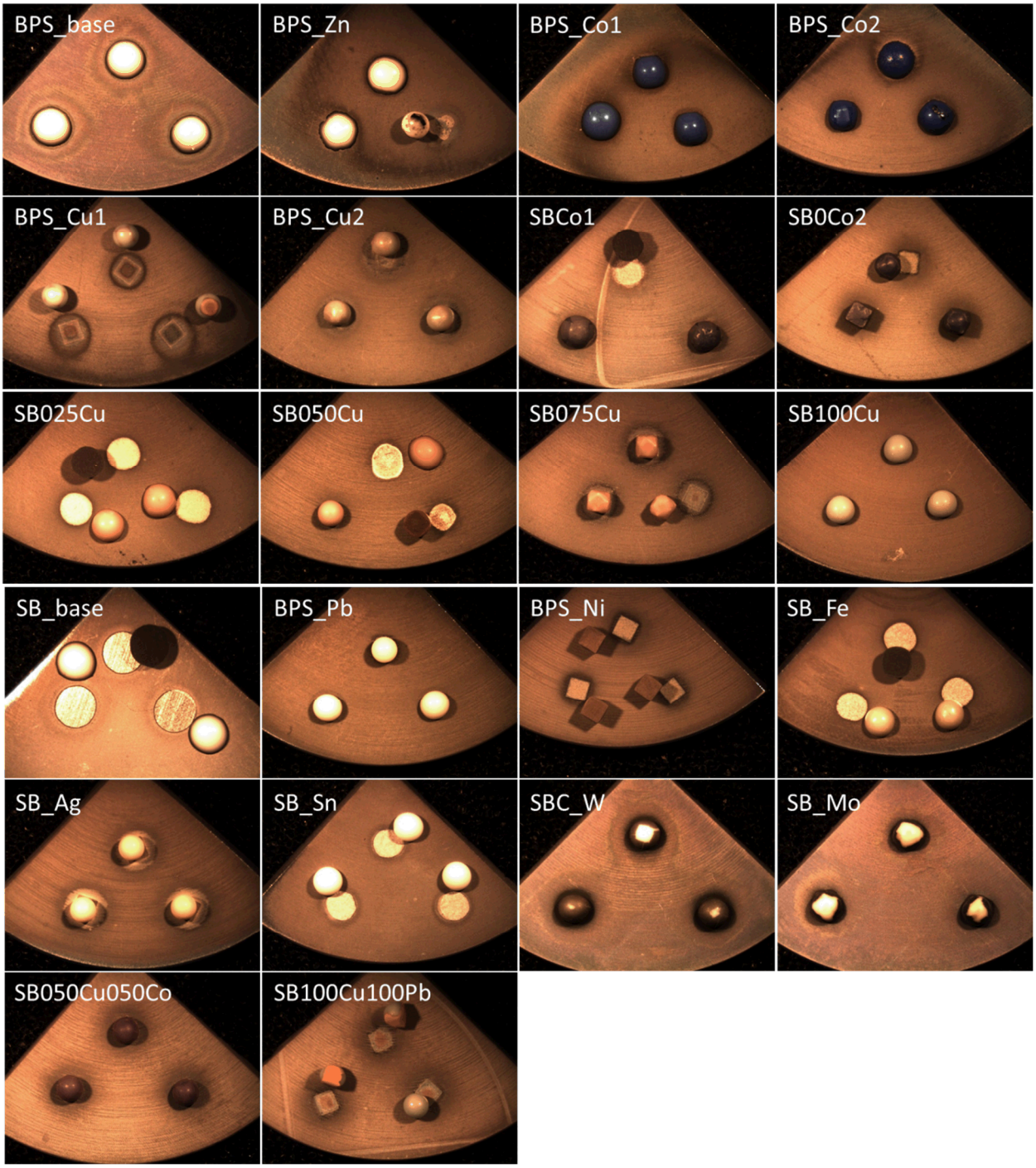

Figure 8. Sessile drop of all glass-ceramic specimens.